# Magnetic Properties and Mössbauer Spectroscopy of Fe_3O_4/$CoFe_2O_4$ Nanorods

Martin Hähsler, Joachim Landers, Tim Nowack, Soma Salamon, Michael Zimmermann, Stefan Heißler, Heiko Wende, and Silke Behrens*

ABSTRACT: Fe_3O_4/$CoFe_2O_4$ nanorods were obtained via a simple seed mediated synthesis. Nanorods were used as seeds to grow $CoFe_2O_4$ by thermal codecomposition of the cobalt(II) and iron(III) acetylacetonate precursors. The growth process was monitored by electron microscopy (SEM, TEM), and the resulting nanorods were characterized by powder X ray diffraction analysis and IR and Raman spectroscopy. Magnetometry and AC susceptometry studies revealed a distribution of Néel relaxation times with an average blocking temperature of 140 K and a high field magnetization of 42 Am^2/kg. Complementarily recorded [57]Fe−Mössbauer spectra were consistent with the Fe_3O_4/$CoFe_2O_4$ spinel structure and exhibited considerable signs of spin frustration, which was correlated to the internal and surface structure of the nanorods.
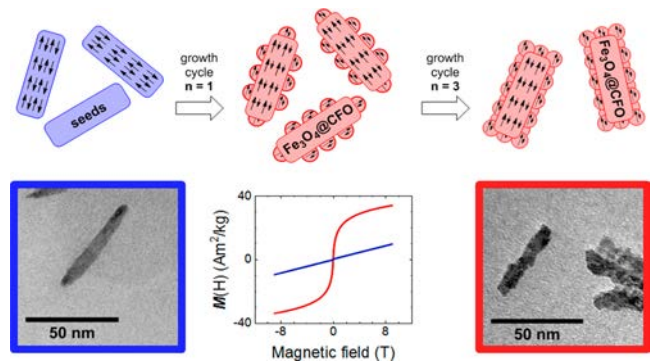
INTRODUCTION

Magnetic nanoparticles (MNPs) reveal interesting size and material dependent properties and have attracted great interest for application in various fields,[1−3] including catalysis,[4,5] theranostics,[6,7] magneto optics,[8−10] and magnetorheology.[11,12] To obtain uniform MNPs with a defined size, shape, and composition, various methods have been established, including cation/anion exchange,[13] coprecipitation,[4,14] thermal decom position,[15−18] microemulsions,[19] and hydrothermal/solvother mal synthesis.[20] In order to obtain monodisperse MNPs, these methods typically separate the nucleation and growth phases into either several temporal or spatial steps.[21] The latter seed mediated growth process usually leads to core/shell nano particles.[22]

$CoFe_2O_4$ (CFO) is a material displaying an inverse spinel structure (i.e., in which Co^{2+} ions preferably occupy the octahedral spinel B sites) and a high chemical and physical stability. The energy for preferential occupation of the octahedral sites in the spinel lattice, however, is relatively small for Co^{2+} compared to other M^{2+} ions. Depending on the synthesis procedure and the number of lattice defects, different degrees of inversion are obtained, i.e., ranging from random Co^{2+} distribution to its preferential occupation of the B site sublattice.[23] Co^{2+} (∼3 μ_B) has a lower atomic magnetic moment than Fe^{3+} (∼5 μ_B), and hence, the magnetic properties will also depend on the degree of inversion. Bulk saturation magnetizations (M_s) of 80 Am^2/kg have been reported for CFO, which is slightly lower than that of

magnetite (Fe_3O_4, M_s ∼89 Am^2/kg), combined with an unusually high magnetocrystalline anisotropy of ∼2 × 10^5 J/m^3.[24] In $Co_xFe_{2−x}O_4$, the magnetocrystalline anisotropy depends on the level of Co^{2+} doping, where larger amounts of Co^{2+} result in higher magnetic anisotropy and coercivity, until a maximum is reached at approximately $x = 0.6$.[25,26] The Curie temperature (T_C) for CFO nanoparticles is about 670 K and decreases with an increasing level of Co^{2+} doping.[27−29] CFO MNPs are particularly appealing materials for various fields of application, and a variety of procedures has been developed, e.g., for the synthesis of spherical or cube shaped CFO MNPs, finely tuned with respect to size, shape, and Co stoichiometry.[30] Reports on the preparation of CFO particles with anisotropic morphology such as nanorods or nanowires, however, are scarce, although the anisotropic MNPs have promising advantages over the spherical shape (e.g., the stronger induced magnetic field).[31] CFO based nanorods should show an M_s comparable to Fe_3O_4; however, the coercivity and the magnetic blocking temperature (T_B) should be significantly increased due to a higher spin−orbit coupling. Due to the symmetric, cubic crystal structure of CFO, it seems to be challenging to control the anisotropic growth of CFO

into small, rod like structures. In order to break the structural symmetry, polymers or soft, micellar templates have been employed to induce anisotropic CFO growth. Large CFO nanowires with widths of 100 nm, for example, were prepared via a sol−gel approach using poly(vinylpyrrolidone) as a surfactant.[32] CFO nanowires with lengths of several micro meters were also synthesized via microemulsion techniques.[33] Hydrothermal synthesis led to bundles of CFO nanorods with a length of 120 nm.[34] Rod like CFO MNPs (lengths 80−160 nm; average width 43 nm) were obtained by coprecipitation and subsequent annealing, in the presence of some remaining spherical MNPs.[35] In general, these procedures typically result in the formation of rather large CFO rods, and to the best of our knowledge, no synthetic routes are available for CFO based nanorods with dimensions in the lower nanometer range (1−100 nm).

In the present work, we address the seed mediated synthesis of small, 51 nm long $Fe_3O_4/CoFe_2O_4$ nanorods, where nanorods of well defined size and shape were used as seeds to direct the epitaxial growth of CFO. The structure and magnetic properties of the seeds and the Fe_3O_4/CFO nanorods were characterized via scanning and transmission electron microscopy (SEM, TEM), powder X ray diffraction analysis (XRD), IR and Raman spectroscopy, field and temperature dependent magnetization measurements follow ing the zero field cooled field cooled (ZFC FC) protocol, and temperature dependent Mössbauer spectroscopy (T = 4.3− 293 K), including experiments in external magnetic fields. The influence of the CFO layer on the magnetic properties was investigated.

EXPERIMENTAL PROCEDURES

Chemicals. Acetone anhydrous (99.9%), cobalt(II) acetylaceto nate ($Co(acac)_2$, 97%), diphenyl ether (99%), 1,2 hexadecandiol (90%), hexadecylamine (99%), n hexane anhydrous (95%), iron(III) acetylacetonate ($Fe(acac)_3$, 97%), iron(0) pentacarbonyl ($Fe(CO)_5$, 99.999%), 1 octanol (99%), oleic acid (90%), and oleylamine (70%) were purchased from Sigma Aldrich GmbH (Steinheim, Germany). Ethanol (99%) was purchased from Merck Chemicals GmbH (Darmstadt). All chemicals were used as received.

Synthesis of Seeds. Hexadecylamine (0.20 g) and oleic acid (2.00 mL) were dissolved in 1 octanol (8 mL) at 50 °C. After 10 min while stirring at 50 °C, the solution was cooled to ambient conditions and transferred to an autoclave reactor (20 mL, PTFE inlet), and $Fe(CO)_5$ (2.10 mL) was added. The autoclave was closed and transferred into an oven, and the heating program was started (20− 200 °C in 2 h, 200 °C for 6 h). Under ambient conditions, ethanol (30 mL) was added to precipitate the crude product of MNPs. The MNPs were washed three times with ethanol (each 15 mL, 500 rcf, 1.5 min). Pure seeds were obtained as a colloidal suspension after the addition of chloroform (20 mL, ca. 6 mg mL^{-1}) and removal of spherical magnetite agglomerates by centrifugation.

Synthesis of Fe_3O_4/CFO Nanorods. $Co(acac)_2$ (257 mg), $Fe(acac)_3$ (706 mg), 1,2 hexadecanediol (2.58 g), oleic acid (1.90 mL), oleylamine (1.97 mL), diphenyl ether (20 mL), and seeds (20 mL of colloidal suspension) were transferred into a 100 mL, three neck, round bottom flask equipped with a condenser and argon inlet and stirred mechanically (800 rpm). The solution was heated using the following heating protocol: (1) 20 to 100 °C (heating rate 7.5 °C min^{-1}), (2) 100 °C (30 min), (3) 100 to 200 °C (heating rate 7.5 °C min^{-1}), (4) 200 °C (30 min), (5) 200 to 230 °C (heating rate 7.5 °C min^{-1}), and (6) 230 °C (30 min). The argon supply was closed at 100 °C. After cooling to room temperature, ethanol (50 mL) was added, and the MNPs were collected via centrifugation (10 min, 4000 rcf). The MNPs were dispersed in n hexane (7.5 mL) containing oleic acid (50 μL)/oleylamine (50 μL). After centrifugation (4000 rcf, 10 min),

the supernatant was collected, and acetone (5 mL) was added. The MNPs were isolated (5 min, 2000 rcf), dispersed in chloroform (7.5 mL), and precipitated again with acetone (5 mL). This washing procedure was repeated five times. In total, this growth procedure was carried out three times.

Characterization. The elemental composition of the MNPs was determined by inductively coupled plasma optical emission spectrometry (ICP OES) with an Agilent 725 ICP OES Spectrometer (Agilent Technologies; USA). For ICP OES analysis, the MNPs were dissolved in hydrochloric acid. Thermal gravimetric analysis was performed on a TGA/SDTA 851e (Mettler Toledo, USA) from 0− 600 °C at a heating rate of 10 °C min^{-1} under a stream of synthetic air (60 mL/min). After deposition on a carbon coated, 400 mesh Cu grid, the size and morphology of the MNPs were analyzed by TEM on an FEI Tecnai F20 ST TEM (operating voltage 200 kV), which was equipped with a field emission gun and EDAX EDS X ray spectrometer and by SEM on a Zeiss GeminiSEM500, equipped with a Schottky type thermal field emission cathode. The particle size and size distribution were determined from TEM images typically based on 300 particles. IR spectra of the samples were recorded as pellets in potassium bromide with a FT IR spectrometer Varian 660 IR (Agilent Technologies, USA). Raman spectra were acquired on a Senterra Raman microscope (Bruker Optics, Ettlingen, Germany). As an excitation source, a frequency doubled Nd:YAG laser (λ = 532 nm) operated at 5 mW output power was used. For observation of the samples, focusing the laser, and collecting the backscattered light, an MPLAN 20× objective, NA 0.45 (Olympus, Tokyo, Japan), was applied. Spectra were measured over 60 s with three coadditions (3 × 20s). Powder XRD measurements were performed with a PANalytical X'Pert Pro X ray diffractometer employing Bragg−Brentano geometry with Cu Kα radiation and a Ni filter. The diffractograms were recorded over a period lasting 16 h at room temperature. The reflections were compared to reference data reported in the Joint Committee of Powder Diffraction Standards (JCPD) database. Magnetization measurements were performed at 5−400 K and 10 mT following the zero field cooled field cooled protocol and field dependently at 5 and 300 K and field amplitudes up to 9 T to study the particles' relaxation dynamics and static magnetic properties using the vibrating sample magnetometer (VSM) option of a Quantum Design PPMS DynaCool. To study nanoparticle relaxation behavior more closely, the nanorods were dispersed in Edwards L9/LP4/ KoratinSH (volume ratio 18/1/1) for an in depth AC susceptometry analysis at temperatures of 5−330 K in 10 K steps and frequencies of 0.1−1500 Hz using eight equidistant frequencies per magnitude with a Quantum Design MPMS 5S SQUID magnetometer with an integrated AC option. Mössbauer spectra were recorded in trans mission geometry and constant acceleration mode utilizing 20−70 mCi ^{57}Co(Rh) sources. A l He bath cryostat was used to attain temperatures of 4.8−300 K and record spectra without external fields to study the sample's general structure and magnetic phase transitions, while a reference spectrum of the dispersed nanorod sample was recorded at 4.8 K in a magnetic field of 5 T applied parallel to the γ ray propagation direction to obtain more detailed information regarding magnetic structure and spin canting effects.

RESULTS AND DISCUSSION

Synthesis of Magnetic Nanorods. The Fe_3O_4/CFO nanorods were synthesized by several steps of seed mediated growth. Initially, the seeds were prepared by decomposition of iron pentacarbonyl according to a procedure previously described by others.[36,37] This procedure results in a mixture of the elongated target seeds and large spherical Fe_3O_4 MNPs.[36] These 50−500 nm spherical MNPs have a M_s of 75 Am^2/kg, whereas the M_s of the seeds is 0.5 Am^2/kg and rather low. It is important to note that the procedure was optimized here to yield exclusively the target seeds as a pure product and no spherical MNPs. Figure 1A and B show the corresponding SEM and TEM micrographs of the pure seeds.

The mean size of the seeds is 57.2 ($\pm$17.8) nm $\times$ 7.1 ($\pm$2.5) nm.
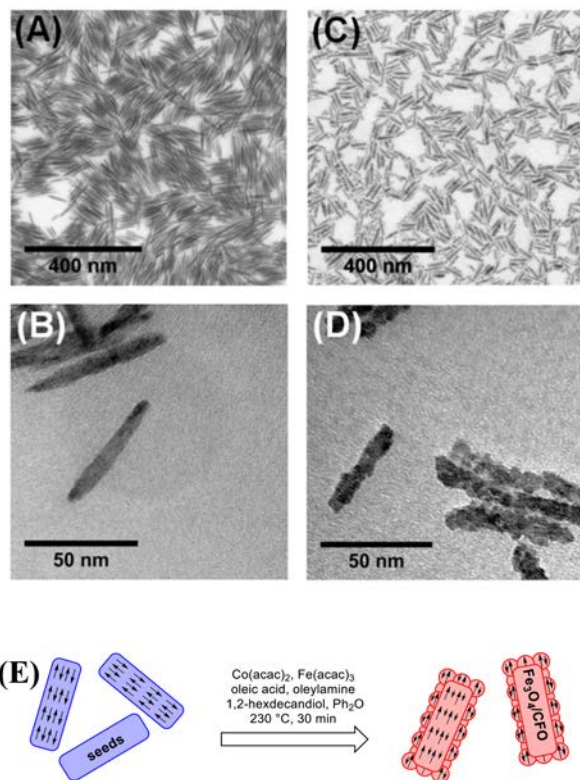
Figure 1. (A) SEM and (B) TEM images of 57.2 $\times$ 7.1 nm seeds and (C) SEM and (D) TEM images of 51.2 $\times$ 9.5 nm Fe$_3$O$_4$/CFO nanorods. (E) Schematic representation for the synthesis of Fe$_3$O$_4$/CFO nanorods.

The seeds were then employed to obtain the Fe$_3$O$_4$/CFO nanorods via decomposition of the iron(III) acetylacetonate and cobalt(II) acetylacetonate precursors.[15] At temperatures above 240 °C, the seeds were transformed into spherical MNPs, and thus, it is important to keep the reaction temperature below 240 °C during CFO coating. It was previously shown that the thermal decomposition of Fe(III) and Co(II) acetylacetonate precursors in high boiling point solvents yields CoFe$_2$O$_4$ particles with high M_s.[38] In our case, however, one growth cycle neither resulted in a thick CFO layer nor did it significantly improve the magnetic properties of the nanorods. An increase in temperature may result in the growth of thicker CFO layers, but as mentioned above, the nanorods decompose into spherical MNPs at higher temperatures.[39]

Therefore, the CFO growth procedure was consecutively repeated three times to obtain nanorods with a distinct CFO layer. Any small spherical MNPs, which formed as byproducts during CFO growth, were separated from the Fe$_3$O$_4$/CFO nanorods via size selective precipitation in consecutive steps of suspension in chloroform and precipitation with acetone. Size selective precipitation techniques have been previously reported to narrow the size distribution of nanoparticles.[40] In this procedure, an antisolvent is added to the suspended MNPs, leading to destabilization and precipitation of larger particles while the smaller ones remain in suspension. Figure 1C and D show the corresponding SEM and TEM images of

the Fe$_3$O$_4$/CFO nanorods. The mean size of the Fe$_3$O$_4$/CFO nanorods is 51.2 ($\pm$16.5) nm $\times$ 9.5 ($\pm$2.2) nm.

Characterization via ICP-OES, XRD, IR, and Raman Spectroscopy. After three cycles of CFO coating, the Fe$_3$O$_4$/CFO nanorods seemed to be slightly shorter than their original seeds, which might be a consequence of the nanorod workup after synthesis. The Co and Fe content of the Fe$_3$O$_4$/CFO nanorods was determined by ICP OES analysis to 13.1 and 48.0 wt %, respectively. This was further supported by SEM EDX analysis. It has to be noted that the original seeds contained only iron (29.6 wt %).

XRD analysis of the Fe$_3$O$_4$/CFO nanorods reveals broad reflections of low intensity, which are characteristic for small, rod like nanoparticles (Figure 2 A). The Fe$_3$O$_4$/CFO nano
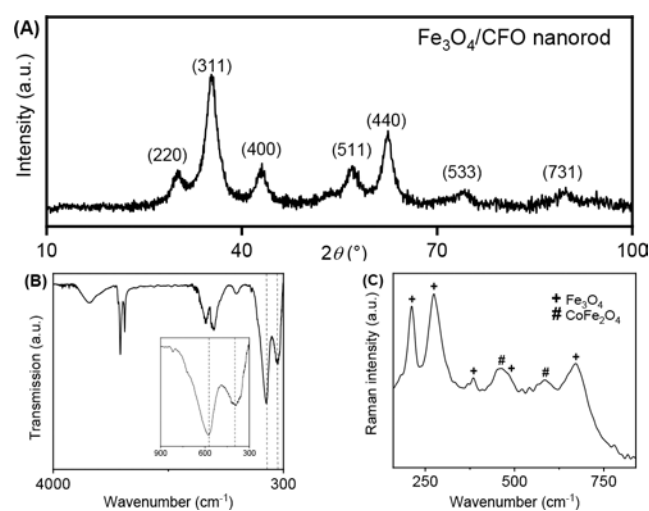
Figure 2. Characterization of Fe$_3$O$_4$/CFO nanorods. (A) The XRD pattern and (B) the IR spectrum reveal the reflections and bands, accordingly, which are characteristic for Fe or Co ferrite. (C) The Raman spectrum shows the characteristic bands of Fe$_3$O$_4$ and CoFe$_2$O$_4$, suggesting that the nanorods are composed of both Fe$_3$O$_4$ and CoFe$_2$O$_4$.

rods show the reflections characteristic of the cubic Fe$_3$O$_4$ or CoFe$_2$O$_4$ phase, which are similar in lattice constants (JCPD 03 065 3107 or JCPD 00 022 1086: 30.1° (220), 35.4° (311), 43.1° (400), 57.0° (511), 62.6° (440), 74.0° (533), 89.7° (731) (2θ)).[28,41] No reflections remain unassigned, which indicates that the Fe$_3$O$_4$/CFO nanorods are indeed composed of ferrite (Fe$_3$O$_4$ and/or CoFe$_2$O$_4$). The diffractograms of the initial seeds revealed broad reflections of low intensity at 17°, 34° (major reflection), 39°, 41°, 46°, 52°, 61°, 71°, and 82° (2θ), which could not be assigned to any of the known ferrite or ferri/ferro (oxide)hydroxide phases and disappeared after CFO coating.[42] This was also the case if the initial seeds were treated under coating conditions but in absence of any additional metal precursors, where reduction to Fe$_3$O$_4$ occurred. In this case, the seeds transformed into Fe$_3$O$_4$ nanorods exhibiting a similar structure to that of the Fe$_3$O$_4$/CFO nanorods but smaller dimensions (for TEM images, XRD analysis, and IR spectra of pure Fe$_3$O$_4$ nanorods as compared to seeds, see SI Figure S2). XRD patterns of the Fe$_3$O$_4$/CFO nanorods and the seeds (without baseline corrections) are displayed in Figure S1B. The increase in background with the Bragg angle (2θ) for Fe$_3$O$_4$/CFO nanorods is due to fluorescence of Co and further supports the formation of CFO. Broad reflections of low intensity in addition to very
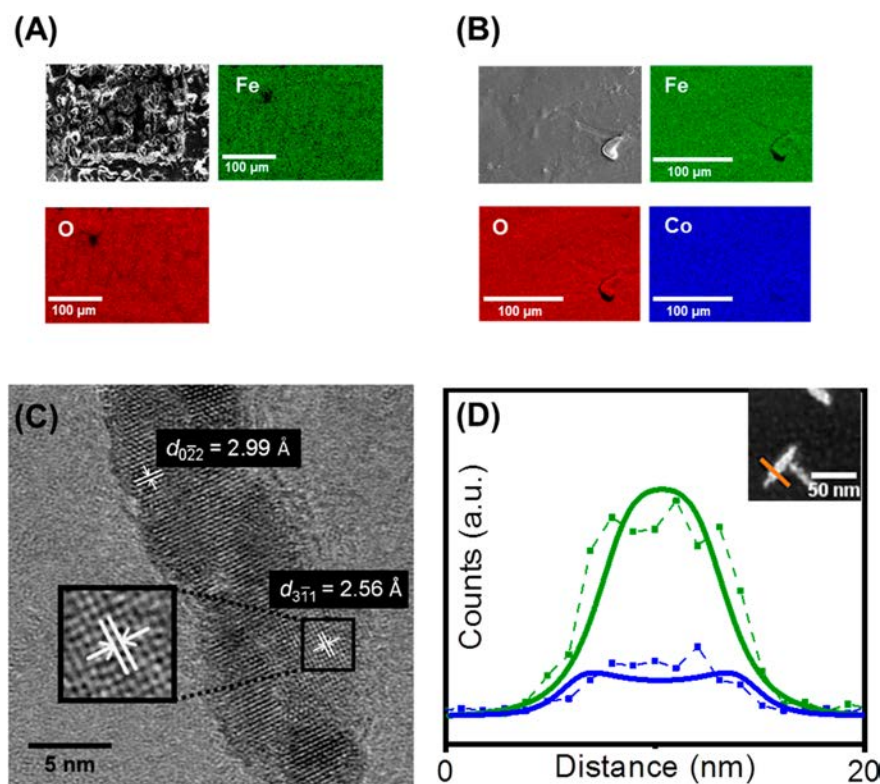
Figure 3. SEM EDX mapping of (A) seeds and (B) Fe_3O_4/CFO nanorods indicating the homogeneous distribution of the elements and the presence of Co after coating (Fe (green), Co (blue), and O (red)). (C) HRTEM micrograph of a Fe_3O_4/CFO nanorod revealing its polycrystalline structure. The lattice spacings are 2.99 and 2.56 Å, which are in good agreement with the (220) and (311) planes of a ferrite phase (either Fe_3O_4 or $CoFe_2O_4$), respectively. (D) EDX line profile showing the distribution of Fe (green) and Co (blue) over the diameter of a single Fe_3O_4/CFO nanorod (inset, red line). Fe and Co distribution over the nanorod diameter indicates a Fe_3O_4 core/$Co_xFe_{3-x}O_4$ shell structure of the nanorods (inset: high angle annular dark field STEM image (HAADF STEM) of Fe_3O_4/CFO nanorod).

similar lattice parameters of Fe_3O_4 and $Co_xFe_{3-x}O_4$ further prevent a detailed phase analysis by XRD. Any amorphous components, which may potentially form during CFO coating of the seeds, may also not be determined by XRD analysis. Therefore, Mössbauer, IR, and Raman spectroscopy as well as electron microscopy with elemental analysis (EDX) were additionally carried out to characterize the structure and composition of the CFO coated nanorods.

The IR spectrum of Fe_3O_4/CFO nanorods shows two protruding bands for the lattice vibration at 578 and 381 cm^{-1} (Figure 2B). Since these bands can be assigned to both ferrites, i.e., Co ferrite (575 cm^{-1}/374 cm^{-1}) and Fe ferrite (570 cm^{-1}/370−380 cm^{-1}), it is not possible to clearly identify the ferrite phase of the Fe_3O_4/CFO nanorods using IR spectroscopy alone.[43] However, complementary Raman analysis confirmed the presence of both ferrites (i.e., Fe_3O_4 and $CoFe_2O_4$) in the Fe_3O_4/CFO nanorods. The Raman spectrum reveals the four bands at 661, 382, 273, and 221 cm^{-1} characteristic for Fe_3O_4 in addition to two bands at 624 and 467 cm^{-1} characteristic for Co ferrite (Figure 2C),[44] indicating both the reduction of the initial nanorod seeds to Fe_3O_4 and their successive coating with CFO.

Electron Microscopy. High resolution transmission electron microscopy (HRTEM), high angle annular dark field−scanning transmission electron microscopy (HAADF STEM), and SEM in combination with elemental analysis (EDX) were employed to further investigate the structure and spatial composition of the nanorods. Elemental maps of both the seeds and the Fe_3O_4/CFO nanorods by SEM EDX also

show the overall presence of cobalt in the Fe_3O_4/CFO nanorods (Figure 3A and B). TEM and SEM images of the seeds and the Fe_3O_4/CFO nanorods are displayed in Figure 1. HRTEM images (Figure 3C) reveal the polycrystalline structure of the Fe_3O_4/CFO nanorods. The lattice fringes are clearly visible, indicating their overall good crystallinity. The lattice spacings are 2.99 and 2.56 Å, which is in good agreement with the (220) and (311) planes of a Fe_3O_4 (JCPD 03 065 3107) or $CoFe_2O_4$ (JCPD 00 022 1086) phase, respectively. Since the Fe_3O_4 and CFO phases have similar lattice parameters and TEM contrast, the two phases cannot be distinguished by HRTEM.[45−47] The EDX line profile of a single Fe_3O_4/CFO nanorod is shown in Figure 3D. As determined by ICP OES analysis, the overall Co and Fe contents in the Fe_3O_4/CFO nanorods were 13.1 and 48.0 wt %, respectively, and thus, the EDX signal expected for Co in a single nanorod is very low. The blue and green lines (Figure 3D) represent the theoretical Co and Fe distribution calculated for a nanorod with Fe_3O_4 core/CFO shell structure and comparable dimensions considering its morphological unevenness and the resolution limit of the electron beam. This EDX profile was calculated based on a 7.1 nm size Fe_3O_4 core and a 1.3 nm thick shell, as determined by TEM microscopy (Figure 1). Assuming such a Fe_3O_4 core/CFO shell structure, an overall atomic Co/Fe ratio of 1:4.5 is calculated for these nanorod dimensions. Blue and green squares indicate the experimental Co and Fe distribution measured by EDX analysis over the diameter of the Fe_3O_4/CFO nanorod (also dashed lines) and may suggest indeed a Fe_3O_4 core/
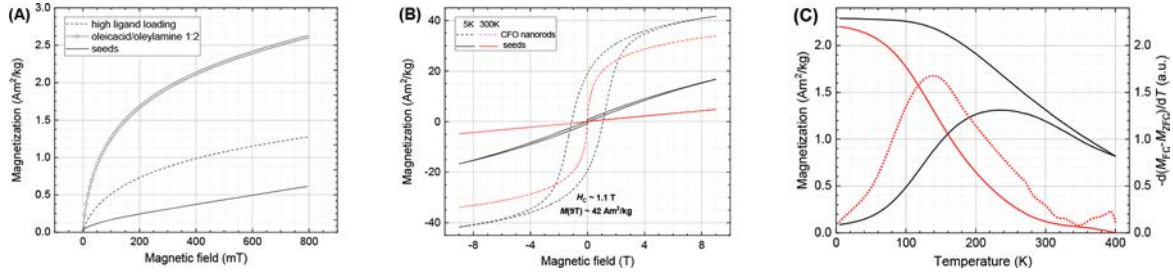
Figure 4. (A)–(B) Field dependent magnetization curves. (A) Influence of reaction parameters on the magnetic properties for one cycle of CFO growth (T = 293 K). (B) M(H) for seed particles (T = 5 K, 300 K, solid line) and for Fe_3O_4/CFO nanorods for three cycles of CFO growth (dashed line). (C) ZFC FC magnetization curves of Fe_3O_4/CFO nanorods (black), difference curve $m_{FC}-m_{ZFC}$ (red, solid) and the differentiated difference curve (red, dotted).

$Co_xFe_{3-x}O_4$ shell structure for the Fe_3O_4/CFO nanorods. This is also in good agreement with the results of Raman spectroscopy showing the presence of both Fe_3O_4 and CFO in the Fe_3O_4/CFO nanorods. The overall Co content of the rods based on the ICP OES analysis (Co/Fe = 1:3.9) seemed to be slightly increased as compared to the theoretical Co content of a 7.1 nm size Fe_3O_4 core/1.3 nm thick CFO shell structure, which could suggest some minor insertion of Co^{2+} in the Fe_3O_4 core. Postsynthetic cation exchange of Fe^{2+} to Co^{2+} was previously reported for Fe_3O_4 nanocrystals.[13]

Magnetic Properties. It is well known that the reaction parameters, e.g. the ligand concentration and the ligand to particle ratio, affect not only the morphology but also the properties of core/shell nanoparticles.[48,49] Therefore, the influence of the ligand on the particle morphology and M_s was further investigated. While the reduction of the ligand concentration by half led to insoluble agglomerates, the doubling yielded nanorods, which were not only soluble in chloroform and n hexane but also showed a slightly increased M_s at 293 K compared to the seeds. The ratio of oleic acid to oleylamine was also important: The nanorods behaved identically within the error of measurement in terms of morphology and M_s, when a ratio of >1 was employed, whereas those obtained with an oleic acid/oleylamine ratio of 1:2 showed a significant increase in M_s (see Figure 4A). As determined by TGA measurements, 30 and 21 wt % organic ligands remained adsorbed on the seeds and the CFO coated particles after synthesis, respectively. Considering the organic residues on the MNP surface, the magnetization data were normalized to estimate the magnetization of the inorganic particle core.

In order to gain a deeper insight into the structure and magnetic behavior, the Fe_3O_4/CFO nanorods were charac terized via field dependent magnetization curves, ZFC/FC curves, and Mössbauer spectroscopy. Fe_3O_4/CFO nanorods showed a broad magnetic hysteresis at 5 K with a coercive field of approximately 1.1 T, as is common for CFO nanoparticles, and a high field magnetization $M_{(9T)}$ of approximately 42 Am^2/kg (Figure 4B), considerably higher than that of the untreated seed material, shown for comparison. The large specific surface and interface area of the Fe_3O_4/CFO nanorods (e.g., due to the polycrystalline and/or core/shell structure) may lead to considerable frustration of spins and reduce the particles' magnetization significantly compared to bulk CFO and magnetite. ZFC FC curves of the Fe_3O_4/CFO nanorods are shown in Figure 4C (black) together with the difference curve $m_{FC}-m_{ZFC}$ (red, solid line) and the differentiated difference curve (red, dotted line), often assumed to be indicative of the

distribution of blocking temperatures $P(T_B)$ as described by[50,51]

$$P(T_B) \propto -\frac{d(m_{FC} - m_{ZFC})}{dT}$$

The observed curves are characteristic for the transition from magnetically blocked to superparamagnetic behavior, with a T_B of approximately 140 K, marked by the inflection point in the ZFC−FC difference magnetization curve.[51] However, a minor splitting of FC and ZFC magnetization up to approximately 400 K indicates a small fraction of particles with higher T_B.

To get a better understanding of magnetic relaxation processes and the distribution of relaxation times, and to test the possibility of future experiments on nanorods in fluid media, the Fe_3O_4/CFO nanorods were dispersed in an organic carrier medium (i.e., Edwards L9) using LP4/KoratinSH (volume ratio 18/1/1) to yield a ferrofluid of 1.1 wt % ferrite nanoparticle concentration. A mapping of the imaginary part χ'' of the magnetic AC susceptibility of the sample fluid was obtained via measurements with a high point density in frequency and temperature (Figure 5), as described in the
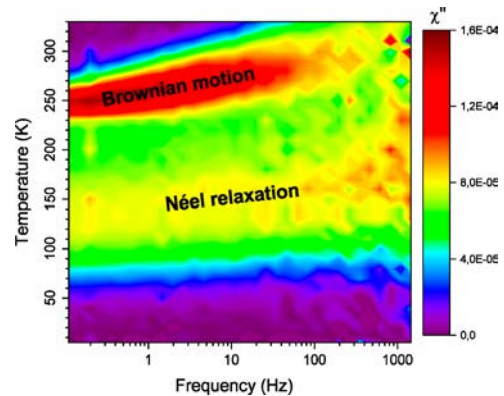
Figure 5. Color map of the imaginary part of AC magnetic susceptibility χ'' (5−330 K, 10 K per step, and 0.1−1500 Hz, 8 steps per magnitude). The signal was interpolated between the experimental data points.

Experimental Procedures. As now spatial rotation of the particles is enabled in the fluid via Brownian particle motion, in addition to the Néel type relaxation of particle superspins, two major streak like features are visible, corresponding to the peaks in more common frequency dependent AC measure ments, representing the relaxation time of magnetic moments in the system at hand at a defined temperature.[52] While the

Fe₃O₄/CFO nanorods are completely magnetically blocked up to ca. 70 K, a broad distribution of different relaxation times is visible at higher temperatures. As the solution can be considered an amorphous solid until much higher temperatures, preventing any magnetic realignment via spatial particle rotation, this contribution can be assigned to Néel type relaxation of the particle magnetic moments. A maximum of this distribution is visible at approximately 140 K, matching the inflection point of the difference curve (red, solid line) in ZFC−FC experiments (Figure 4C). Although it is hard to assign a specific time constant to the ZFC−FC experiment, to allow for comparison to blocking temperatures studied in AC susceptometry, the general agreement of T_B observed in magnetization measurements of the nanoparticle powder and AC susceptometry of the dissolved nanoparticles indicates the absence of strong magnetic interparticle interaction, which would lead to a considerably increased blocking temperature for the powder sample. This could be explained by a diminished net magnetization, especially of the outer regions of the nanorods, caused by strong spin frustration (inferred from in field Mössbauer spectroscopy discussed in the following section) likely to be located at internal interfaces, as well as at the particle surface, as the somewhat irregular surface geometry may result in an enhanced specific surface area of the particles.

In Figure 5, an additional streak appears at approximately 250 K, representing the realignment of the particle magnetic moments via spatial particle rotation on the frequency scale of our experiments, as the solution reaches sufficiently low viscosities. Particles, which are still magnetically blocked in terms of Néel relaxation, now also display a quasi super paramagnetic behavior enabled by the onset of Brownian particle motion, resulting in similar magnetization dynamics on the time scale of the measurement method, although it is of course based on a different physical mechanism.

Mössbauer Spectroscopy. Complementary Mössbauer experiments were performed to analyze the magnetic structure of the particles' individual components and their magnetic alignment behavior. Mössbauer spectra of the nanoparticle powder (Figure 6) as well as the seed crystals (Figure S3) were recorded at temperatures down to 4.3 K. In the case of untreated seed crystals, the presence of Fe^{3+} and Fe^{2+} states in Mössbauer spectra show a transition to an ordered sextet structure at similar temperatures of ca. 30−40 K, which could indicate a Fe hydroxide/carbonate phase (e.g., partially oxidized green rust $(Fe_{6-x}^{3+}Fe_x^{2+}O_{4-x}(OH)_{8+x}(CO_3)\cdot 3H_2O)^{42}$ or siderite $(FeCO_3)$, both showing matching ordering temperatures,[53] possibly in a mixture with Fe^{3+} bearing six line ferrihydrite. CO_3^{2-} may form during seed synthesis from $Fe(CO)_5$ under solvothermal conditions. However, a clear assignment to either of these Fe hydroxide/carbonate phases was not possible based on the IR spectra.

Mössbauer spectra of the Fe₃O₄/CFO nanorod powder, on the other hand, display superparamagnetic properties: Upon rising temperature, a significant superparamagnetic contribution is visible, containing about 30% of spectral area (olive) at room temperature. The remaining fraction of magnetically blocked CFO and Fe₃O₄ displays a sextet subspectrum with broad inner shoulders (violet), caused by beginning super paramagnetic relaxation, preventing the resolution of individual contributions of spinel tetrahedral A and octahedral B sites at elevated temperatures. The apparent contradiction to blocking temperatures as determined in magnetometry and suscep
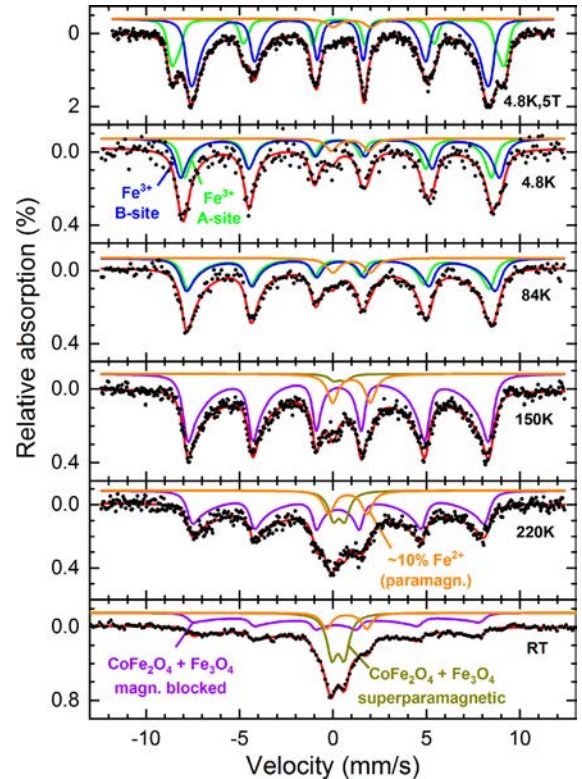
Figure 6. Mössbauer spectra of Fe₃O₄/CFO nanorods recorded at 4.8 K up to room temperature (RT), containing Fe^{3+} on octahedral B sites (blue) and tetrahedral A sites (green) in $CoFe_2O_4$ and Fe_3O_4. Upon rising temperature, A and B sites cannot be resolved, whereby the spectrum is divided into a magnetically blocked (violet) and superparamagnetic (olive) fraction. Also visible is a minor contribution assigned to paramagnetic Fe^{2+} (orange). The spectrum recorded in an external magnetic field of 5 T applied parallel to the γ ray direction is shown for comparison (top), to illustrate the in field alignment behavior of the nanorods. To account for the effects of broadened absorption lines and distinct spin frustration, the experimental spectrum has been reproduced using hyperfine field sextet distributions.

tometry experiments can be explained by the much shorter time window of the Mössbauer technique.[55] Also barely visible is a minor doublet subspectrum, whose high isomer shift (ca. 0.84 mm/s measured at room temperature relative to α Fe) and quadrupole splitting (2.16 mm/s) indicate a minor Fe^{2+} phase (ca. 10% of spectral area), probably remaining from the original seed material. At lower temperatures the super paramagnetic doublet decreases in intensity, while the sextet increases in area and becomes more symmetric, as the lower thermal energy is insufficient to excite fast superspin fluctuation, whereby the magnetically blocked spectral contribution can be resolved into Fe^{3+} on A (green) and B site subspectra (blue) below ca. 100 K. However, as hyperfine parameters such as the hyperfine magnetic field B_{hf} as well as the isomer shift of the respective lattice position in $CoFe_2O_4$ and Fe_3O_4 are quite similar[54,55] and the observed sextets being somewhat broadened even at a minimum temperature of 4.8 K, these subspectra cannot be unambiguously resolved into contributions of CFO and Fe_3O_4 to determine their relative composition. We presume this to stem from distributions in B_{hf} of frustrated magnetic states close to interfaces and the particle surface, or the beginning of superparamagnetic relaxation of individual isolated ultrasmall nanocrystals of CFO on the

nanorod surface even at very limited thermal energy. These effects also prevent the possible detection of a minor Fe^{2+} sextet subspectrum, whose presence would be expected assuming ca. 50 wt % Fe_3O_4 core material. Also, a partial oxidation of the nanorod core from magnetite to maghemite (γ-Fe_2O_3) could further lead to a reduced Fe^{2+} content in the particles.

The in field spectrum (Figure 6 top) shows partial splitting between A and B site subspectra, resulting from the different sublattice spin orientations relative to the external magnetic field, as expected for the ferrimagnetic CFO and Fe_3O_4 spinel phases. However, even in an external magnetic field of 5 T (aligned parallel to the γ-ray propagation direction), the sample material displays considerable spin canting, close to a state of random spin orientation, visible via the relatively high intensity of lines no. 2 and 5 in the spectrum, from which an average spin canting angle of ca. 45° relative to the field direction can be inferred.[56] Absorption lines in the in field spectrum are broadened and asymmetric to a certain degree, presumably caused by the superposition of slightly different CFO and Fe_3O_4 subspectral contributions and/or a minor magnetite Fe^{2+} fraction, accounted for by the use of hyperfine field sextet distributions. The observation of considerable canting at 5 T matches the slow rise in field dependent magnetization, as discussed in the previous section, indeed pointing toward a local highly frustrated spin structure rather than to a pronounced decrease in M_s by antiferromagnetic or paramagnetic byproducts, which would be clearly visible in the in field Mössbauer spectrum when present in relevant concentrations. Thereby, we would connect the clearly visible signs of spin frustration to contributions of the iron oxide to cobalt ferrite interface, as well as of the undercoordinated surface atoms,[57−59] as the nanorods' specific surface area may be increased to some degree by the rough surface structure observable for some of the particles in TEM images (Figure 1). Frustrated spin structures may additionally be more likely even within the nanoparticles' core due to the possible presence of structural defects arising from the phase transition of the original seed material to magnetite. The primary origin of spin frustration will be clarified in future investigations by comparing the spin structure of core−shell nanorods of different shell thickness.

CONCLUSION

For the first time, well defined, Fe_3O_4/CFO nanorods were prepared by a seed mediated synthesis with dimensions in the range of 1−100 nm. The Fe_3O_4/CFO nanorods revealed a mean length and width of 51.2 and 9.5 nm, respectively, corresponding to an aspect ratio of 5.4:1. The nanorods were colloidally stabilized in common organic solvents, which is an important aspect for future technical application. The formation of the Fe_3O_4/CFO nanorods was accompanied by a significant increase in M_s—as compared to the original nanorod seeds. ZFC/FC magnetization curves and a detailed AC susceptometry mapping display partial superparamagnetic behavior with an average T_B of ca. 140 K and a broad distribution of Néel relaxation times. A maximum high field magnetization of 42 Am^2/kg was determined by magnetometry at 4.3 K and 9 T. In field Mössbauer experiments demonstrated strong spin frustration in external fields of 5 T, probably located at the CFO surface or the Fe_3O_4/CFO interface, which is assumed to be the primary origin of limited high field magnetization. Further Mössbauer spectroscopy

studies confirmed the expected magnetic spinel structure and blocking temperatures determined via magnetometry and allowed estimation of the amount of an Fe^{2+} containing phase to approximately 10%. Future studies will be directed toward optimization of the CFO shell thickness and homogeneity in order to tune spin frustration effects. Overall, Fe_3O_4/CFO nanorods, investigated in this study, may provide ferrofluids in organic and aqueous carrier media with interesting magnetorheological properties, an aspect which will be another subject of future investigations.

AUTHOR INFORMATION

Corresponding Author

Silke Behrens − *Institute of Catalysis Research and Technology, Karlsruhe Institute of Technology, 76021 Karlsruhe, Germany; Institute of Inorganic Chemistry, Ruprecht Karls University Heidelberg, 69120 Heidelberg, Germany;* orcid.org/0000 0003 4328 9564; Email: silke.behrens@kit.edu

Authors

Martin Hähsler − *Institute of Catalysis Research and Technology, Karlsruhe Institute of Technology, 76021 Karlsruhe, Germany; Institute of Inorganic Chemistry, Ruprecht Karls University Heidelberg, 69120 Heidelberg, Germany;* orcid.org/0000 0002 2352 5286

Joachim Landers − *Faculty of Physics and Center for Nanointegration Duisburg Essen (CENIDE), University of Duisburg Essen, 47057 Duisburg, Germany;* orcid.org/0000 0002 4506 6383

Tim Nowack − *Institute of Inorganic Chemistry, Ruprecht Karls University Heidelberg, 69120 Heidelberg, Germany*

Soma Salamon − *Faculty of Physics and Center for Nanointegration Duisburg Essen (CENIDE), University of Duisburg Essen, 47057 Duisburg, Germany;* orcid.org/0000 0002 8661 6038

Michael Zimmermann − *Institute of Catalysis Research and Technology, Karlsruhe Institute of Technology, 76021 Karlsruhe, Germany*

Stefan Heißler − *Institute of Functional Interfaces, Karlsruhe Institute of Technology, 76021 Karlsruhe, Germany*

Heiko Wende − *Faculty of Physics and Center for Nanointegration Duisburg Essen (CENIDE), University of Duisburg Essen, 47057 Duisburg, Germany;* orcid.org/0000 0001 8395 3541

REFERENCES

(1) Lu, A. H.; Salabas, E. L.; Schüth, F. Magnetic Nanoparticles: Synthesis, Protection, Functionalization, and Application. *Angew. Chem., Int. Ed.* **2007**, *46* (8), 1222−1244.

(2) Behrens, S.; Appel, I. Magnetic nanocomposites. *Curr. Opin. Biotechnol.* **2016**, *39*, 89−96.

(3) Behrens, S. Preparation of functional magnetic nanocomposites and hybrid materials: recent progress and future directions. *Nanoscale* **2011**, *3* (3), 877−892.

(4) Lu, A. H.; Schmidt, W.; Matoussevitch, N.; Bönnemann, H.; Spliethoff, B.; Tesche, B.; Bill, E.; Kiefer, W.; Schüth, F. Nano engineering of a Magnetically Separable Hydrogenation Catalyst. *Angew. Chem., Int. Ed.* **2004**, *43* (33), 4303−4306.

(5) Polshettiwar, V.; Luque, R.; Fihri, A.; Zhu, H.; Bouhrara, M.; Basset, J. M. Magnetically Recoverable Nanocatalysts. *Chem. Rev.* **2011**, *111* (5), 3036−3075.

(6) Behrens, S.; Bönnemann, H.; Matoussevitch, N.; Gorschinski, A.; Dinjus, E.; Habicht, W.; Bolle, J.; Zinoveva, S.; Palina, N.; Hormes, J.; Modrow, H.; Bahr, S.; Kempter, V. Surface engineering of Co and FeCo nanoparticles for biomedical application. *J. Phys.: Condens. Matter* **2006**, *18* (38), S2543.

(7) Barreto, J. A.; O'Malley, W.; Kubeil, M.; Graham, B.; Stephan, H.; Spiccia, L. Nanomaterials: Applications in Cancer Imaging and Therapy. *Adv. Mater.* **2011**, *23* (12), H18−H40.

(8) Xu, Z.; Hou, Y.; Sun, S. Magnetic Core/Shell Fe$_3$O$_4$/Au and Fe$_3$O$_4$/Au/Ag Nanoparticles with Tunable Plasmonic Properties. *J. Am. Chem. Soc.* **2007**, *129* (28), 8698−8699.

(9) Nie, Z.; Petukhova, A.; Kumacheva, E. Properties and emerging applications of self assembled structures made from inorganic nanoparticles. *Nat. Nanotechnol.* **2010**, *5*, 15.

(10) Mertelj, A.; Lisjak, D.; Drofenik, M.; Čopič, M. Ferromagnet ism in suspensions of magnetic platelets in liquid crystal. *Nature* **2013**, *504*, 237.

(11) Chikazumi, S.; Taketomi, S.; Ukita, M.; Mizukami, M.; Miyajima, H.; Setogawa, M.; Kurihara, Y. Physics of magnetic fluids. *J. Magn. Magn. Mater.* **1987**, *65* (2), 245−251.

(12) Odenbach, S.; Thurm, S. Magnetoviscous Effects in Ferrofluids. In *Ferrofluids: Magnetically Controllable Fluids and Their Applications*; Odenbach, S., Ed.; Springer: Berlin, 2002; pp 185−201.

(13) Sytnyk, M.; Kirchschlager, R.; Bodnarchuk, M. I.; Primetzhofer, D.; Kriegner, D.; Enser, H.; Stangl, J.; Bauer, P.; Voith, M.; Hassel, A. W.; Krumeich, F.; Ludwig, F.; Meingast, A.; Kothleitner, G.; Kovalenko, M. V.; Heiss, W. Tuning the Magnetic Properties of Metal Oxide Nanocrystal Heterostructures by Cation Exchange. *Nano Lett.* **2013**, *13* (2), 586−593.

(14) Appel, I.; Nadasi, H.; Reitz, C.; Sebastian, N.; Hahn, H.; Eremin, A.; Stannarius, R.; Behrens, S. S. Doping of nematic cyanobiphenyl liquid crystals with mesogen hybridized magnetic nanoparticles. *Phys. Chem. Chem. Phys.* **2017**, *19*, 12127.

(15) Sun, S.; Zeng, H.; Robinson, D. B.; Raoux, S.; Rice, P. M.; Wang, S. X.; Li, G. Monodisperse MFe$_2$O$_4$ (M = Fe, Co, Mn) Nanoparticles. *J. Am. Chem. Soc.* **2004**, *126* (1), 273−279.

(16) Behrens, S.; Essig, S. A facile procedure for magnetic fluids using room temperature ionic liquids. *J. Mater. Chem.* **2012**, *22* (9), 3811−3816.

(17) Essig, S.; Behrens, S. Ionic Liquids as Size and Shape Regulating Solvents for the Synthesis of Cobalt Nanoparticles. *Chem. Ing. Tech.* **2015**, *87* (12), 1741−1747.

(18) Gorschinski, A.; Khelashvili, G.; Schild, D.; Habicht, W.; Brand, R.; Ghafari, M.; Bönnemann, H.; Dinjus, E.; Behrens, S. A simple aminoalkyl siloxane mediated route to functional magnetic metal nanoparticles and magnetic nanocomposites. *J. Mater. Chem.* **2009**, *19* (46), 8829−8838.

(19) Liu, C.; Zou, B.; Rondinone, A. J.; Zhang, Z. J. Reverse Micelle Synthesis and Characterization of Superparamagnetic MnFe$_2$O$_4$ Spinel Ferrite Nanocrystallites. *J. Phys. Chem. B* **2000**, *104* (6), 1141−1145.

(20) Wang, X.; Zhuang, J.; Peng, Q.; Li, Y. A general strategy for nanocrystal synthesis. *Nature* **2005**, *437*, 121.

(21) LaMer, V. K.; Dinegar, R. H. Theory, Production and Mechanism of Formation of Monodispersed Hydrosols. *J. Am. Chem. Soc.* **1950**, *72* (11), 4847−4854.

(22) Yu, H.; Gibbons, P. C.; Kelton, K. F.; Buhro, W. E. Heterogeneous Seeded Growth: A Potentially General Synthesis of Monodisperse Metallic Nanoparticles. *J. Am. Chem. Soc.* **2001**, *123* (37), 9198−9199.

(23) Navrotsky, A.; Kleppa, O. J. Thermodynamics of formation of simple spinels. *J. Inorg. Nucl. Chem.* **1968**, *30* (2), 479−498.

(24) Sathya, A.; Guardia, P.; Brescia, R.; Silvestri, N.; Pugliese, G.; Nitti, S.; Manna, L.; Pellegrino, T. Co$_x$Fe$_{3−x}$O$_4$ Nanocubes for Theranostic Applications: Effect of Cobalt Content and Particle Size. *Chem. Mater.* **2016**, *28* (6), 1769−1780.

(25) Yu, Y.; Mendoza Garcia, A.; Ning, B.; Sun, S. Cobalt Substituted Magnetite Nanoparticles and Their Assembly into Ferrimagnetic Nanoparticle Arrays. *Adv. Mater.* **2013**, *25* (22), 3090−3094.

(26) Fantechi, E.; Campo, G.; Carta, D.; Corrias, A.; de Julián Fernández, C.; Gatteschi, D.; Innocenti, C.; Pineider, F.; Rugi, F.; Sangregorio, C. Exploring the Effect of Co Doping in Fine Maghemite Nanoparticles. *J. Phys. Chem. C* **2012**, *116* (14), 8261−8270.

(27) Chinnasamy, C. N.; Jeyadevan, B.; Shinoda, K.; Tohji, K.; Djayaprawira, D. J.; Takahashi, M.; Joseyphus, R. J.; Narayanasamy, A. Unusually high coercivity and critical single domain size of nearly monodispersed CoFe$_2$O$_4$ nanoparticles. *Appl. Phys. Lett.* **2003**, *83* (14), 2862−2864.

(28) Zi, Z.; Sun, Y.; Zhu, X.; Yang, Z.; Dai, J.; Song, W. Synthesis and magnetic properties of CoFe$_2$O$_4$ ferrite nanoparticles. *J. Magn. Magn. Mater.* **2009**, *321* (9), 1251−1255.

(29) Houshiar, M.; Zebhi, F.; Razi, Z. J.; Alidoust, A.; Askari, Z. Synthesis of cobalt ferrite (CoFe$_2$O$_4$) nanoparticles using combustion, coprecipitation, and precipitation methods: A comparison study of size, structural, and magnetic properties. *J. Magn. Magn. Mater.* **2014**, *371*, 43−48.

(30) Deng, H.; Li, X.; Peng, Q.; Wang, X.; Chen, J.; Li, Y. Monodisperse Magnetic Single Crystal Ferrite Microspheres. *Angew. Chem., Int. Ed.* **2005**, *44* (18), 2782−2785.

(31) Mohapatra, J.; Mitra, A.; Tyagi, H.; Bahadur, D.; Aslam, M. Iron oxide nanorods as high performance magnetic resonance imaging contrast agents. *Nanoscale* **2015**, *7* (20), 9174−9184.

(32) Wang, Z.; Liu, X.; Lv, M.; Chai, P.; Liu, Y.; Zhou, X.; Meng, J. Preparation of One Dimensional CoFe$_2$O$_4$ Nanostructures and Their Magnetic Properties. *J. Phys. Chem. C* **2008**, *112* (39), 15171−15175.

(33) Zhang, Z.; Rondinone, A. J.; Ma, J. X.; Shen, J.; Dai, S. Morphologically Templated Growth of Aligned Spinel CoFe$_2$O$_4$ Nanorods. *Adv. Mater.* **2005**, *17* (11), 1415−1419.

(34) Ji, G. B.; Tang, S. L.; Ren, S. K.; Zhang, F. M.; Gu, B. X.; Du, Y. W. Simplified synthesis of single crystalline magnetic CoFe$_2$O$_4$ nanorods by a surfactant assisted hydrothermal process. *J. Cryst. Growth* **2004**, *270* (1), 156−161.

(35) Su, K. P.; Zhao, C. Y.; Wang, H. O.; Huang, S.; Liu, Z. W.; Huo, D. X. Synthesis, structure and magnetic properties of $CoFe_2O_4$ ferrite nanoparticles. *Mater. Res. Express* **2018**, *5* (5), 056102.

(36) Sun, H.; Chen, B.; Jiao, X.; Jiang, Z.; Qin, Z.; Chen, D. Solvothermal Synthesis of Tunable Electroactive Magnetite Nanorods by Controlling the Side Reaction. *J. Phys. Chem. C* **2012**, *116* (9), 5476−5481.

(37) Si, J. C.; Xing, Y.; Peng, M. L.; Zhang, C.; Buske, N.; Chen, C.; Cui, C. L. Solvothermal synthesis of tunable iron oxide nanorods and their transfer from organic phase to water phase. *CrystEngComm* **2014**, *16* (4), 512−516.

(38) Fantechi, E.; Innocenti, C.; Albino, M.; Lottini, E.; Sangregorio, C. Influence of cobalt doping on the hyperthermic efficiency of magnetite nanoparticles. *J. Magn. Magn. Mater.* **2015**, *380*, 365−371.

(39) Ghosh Chaudhuri, R.; Paria, S. Core/Shell Nanoparticles: Classes, Properties, Synthesis Mechanisms, Characterization, and Applications. *Chem. Rev.* **2012**, *112* (4), 2373−2433.

(40) Kowalczyk, B.; Lagzi, I.; Grzybowski, B. A. Nanoseparations: Strategies for size and/or shape selective purification of nanoparticles. *Curr. Opin. Colloid Interface Sci.* **2011**, *16* (2), 135−148.

(41) Rajendran, M.; Pullar, R. C.; Bhattacharya, A. K.; Das, D.; Chintalapudi, S. N.; Majumdar, C. K. Magnetic properties of nanocrystalline $CoFe_2O_4$ powders prepared at room temperature: variation with crystallite size. *J. Magn. Magn. Mater.* **2001**, *232* (1), 71−83.

(42) Usman, M.; Byrne, J. M.; Chaudhary, A.; Orsetti, S.; Hanna, K.; Ruby, C.; Kappler, A.; Haderlein, S. B. Magnetite and Green Rust: Synthesis, Properties, and Environmental Applications of Mixed Valent Iron Minerals. *Chem. Rev.* **2018**, *118* (7), 3251−3304.

(43) Waldron, R. D. Infrared Spectra of Ferrites. *Phys. Rev.* **1955**, *99* (6), 1727−1735.

(44) da Silva, S.W.; Melo, T.F.O.; Soler, M.A.G.; Lima, E.C.D.; da Silva, M.F.; Morais, P.C. Stability of citrate coated magnetite and cobalt ferrite nanoparticles under laser irradiation: a Raman spectros copy investigation. *IEEE Trans. Magn.* **2003**, *39* (5), 2645−2647.

(45) Anil Kumar, P.; Ray, S.; Chakraverty, S.; Sarma, D. D. Engineered spin valve type magnetoresistance in Fe_3O_4 $CoFe_2O_4$ core shell nanoparticles. *Appl. Phys. Lett.* **2013**, *103* (10), 102406.

(46) López Ortega, A.; Lottini, E.; Bertoni, G.; de Julián Fernández, C.; Sangregorio, C. Topotaxial Phase Transformation in Cobalt Doped Iron Oxide Core/Shell Hard Magnetic Nanoparticles. *Chem. Mater.* **2017**, *29* (3), 1279−1289.

(47) Lottini, E.; López Ortega, A.; Bertoni, G.; Turner, S.; Meledina, M.; Van Tendeloo, G.; de Julián Fernández, C.; Sangregorio, C. Strongly Exchange Coupled Core|Shell Nanoparticles with High Magnetic Anisotropy: A Strategy toward Rare Earth Free Permanent Magnets. *Chem. Mater.* **2016**, *28* (12), 4214−4222.

(48) Kobayashi, Y.; Horie, M.; Konno, M.; Rodríguez González, B.; Liz Marzán, L. M. Preparation and Properties of Silica Coated Cobalt Nanoparticles. *J. Phys. Chem. B* **2003**, *107* (30), 7420−7425.

(49) Wang; Luo, J.; Fan, Q.; Suzuki, M.; Suzuki, I. S.; Engelhard, M. H.; Lin, Y.; Kim, N.; Wang, J. Q.; Zhong, C. J. Monodispersed Core−Shell Fe_3O_4@Au Nanoparticles. *J. Phys. Chem. B* **2005**, *109* (46), 21593−21601.

(50) Hansen, M. F.; Mørup, S. Estimation of blocking temperatures from ZFC/FC curves. *J. Magn. Magn. Mater.* **1999**, *203* (1), 214−216.

(51) Denardin, J. C.; Brandl, A. L.; Knobel, M.; Panissod, P.; Pakhomov, A. B.; Liu, H.; Zhang, X. X. Thermoremanence and zero field cooled/field cooled magnetization study of $Co_x(SiO_2)_{1-x}$ gran ular films. *Phys. Rev. B: Condens. Matter Mater. Phys.* **2002**, *65* (6), 064422.

(52) Landers, J.; Salamon, S.; Remmer, H.; Ludwig, F.; Wende, H. In Field Orientation and Dynamics of Ferrofluids Studied by Mössbauer Spectroscopy. *ACS Appl. Mater. Interfaces* **2019**, *11* (3), 3160−3168.

(53) Génin, J. M.; Christy, A.; Kuzmann, E.; Mills, S.; Ruby, C. Structure and occurrences of ≪green rust≫ related new minerals of the ≪fougerite≫ group, trébeurdenite and mössbauerite, belonging to the ≪hydrotalcite≫ supergroup; how Mössbauer spectroscopy helps XRD. *Hyperfine Interact.* **2014**, *226*, 459−482.

(54) Arelaro, A. D.; Rossi, L. M.; Rechenberg, H. R. In field Mössbauer characterization of MFe_2O_4 (M = Fe, Co, Ni) nano particles. *Journal of Physics: Conference Series* **2010**, *217*, 012126.

(55) Mørup, S.; Hansen, M. F.; Frandsen, C. 1.14   Magnetic Nanoparticles. In *Comprehensive Nanoscience and Technology*; Andrews, D. L., Scholes, G. D., Wiederrecht, G. P., Eds.; Academic Press: Amsterdam, 2011; pp 437−491.

(56) Glaser, T. Mössbauer Spectroscopy and Transition Metal Chemistry. Fundamentals and Applications. Herausgegeben von Philipp Gütlich, Eckhard Bill und Alfred X. Trautwein. *Angew. Chem.* **2011**, *123* (43), 10195−10196.

(57) Coey, J. M. D. Noncollinear Spin Arrangement in Ultrafine Ferrimagnetic Crystallites. *Phys. Rev. Lett.* **1971**, *27* (17), 1140−1142.

(58) Rechenberg, H. R.; Tourinho, F. A. Mössbauer spectroscopic characterization of manganese and cobalt ferrite ferrofluids. *Hyperfine Interact.* **1991**, *67* (1), 627−631.

(59) Sousa, E. C.; Rechenberg, H. R.; Depeyrot, J.; Gomes, J. A.; Aquino, R.; Tourinho, F. A.; Dupuis, V.; Perzynski, R. In field Mossbauer study of disordered surface spins in core/shell ferrite nanoparticles. *J. Appl. Phys.* **2009**, *106* (9), 093901.

Repository KITopen

Dies ist ein Postprint/begutachtetes Manuskript.

Empfohlene Zitierung:

Hähsler, M.; Landers, J.; Nowack, T.; Salamon, S.; Zimmermann, M.; Heißler, S.; Wende, H.; Behrens, S.
Magnetic Properties and Mössbauer Spectroscopy of Fe3O4/CoFe2O4 Nanorods.
2020. Inorganic chemistry, 59.
doi:10.5445/IR/1000118398

Zitierung der Originalveröffentlichung:

Hähsler, M.; Landers, J.; Nowack, T.; Salamon, S.; Zimmermann, M.; Heißler, S.; Wende, H.; Behrens, S.
Magnetic Properties and Mössbauer Spectroscopy of Fe3O4/CoFe2O4 Nanorods.
2020. Inorganic chemistry, 59 (6), 3677–3685.
doi:10.1021/acs.inorgchem.9b03267